Optimizing Interface Conductivity in Electronics

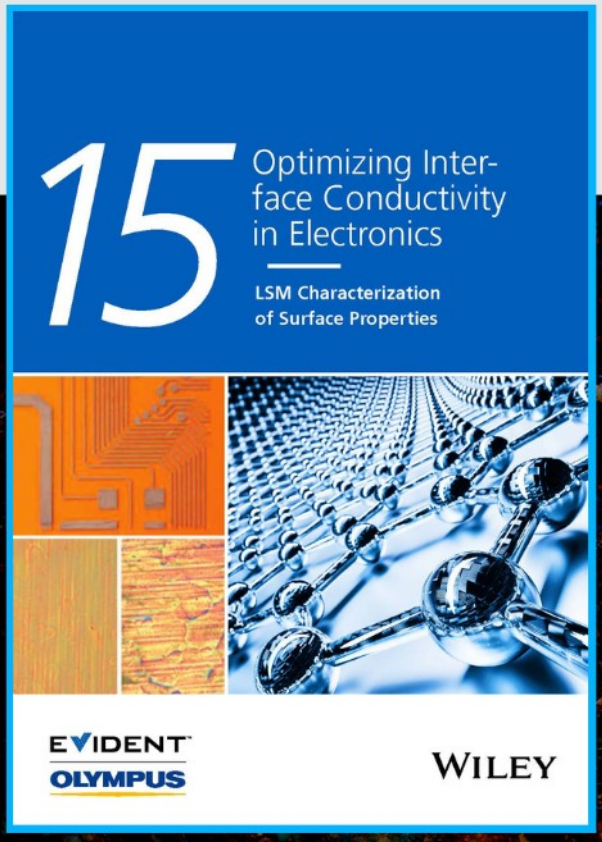

The latest eBook from Advanced Optical Metrology. Download for free.

Surface roughness is a key parameter for judging the performance of a given material's surface quality for its electronic application. A powerful tool to measure surface roughness is 3D laser scanning confocal microscopy (LSM), which will allow you to assess roughness and compare production and finishing methods, and improve these methods based on mathematical models.

Focus on creating high-conductivity electronic devices with minimal power loss using laser scanning microscopy is an effective tool to discern a variety of roughness parameters.

EVIDENT
OLYMPUS

WILEY

ADVANCED FUNCTIONAL MATERIALS
www.afm-journal.de

Highly Flexible and Twistable Freestanding Single Crystalline Magnetite Film with Robust Magnetism

Feng An, Ke Qu, Gaokuo Zhong, Yongqi Dong, Wenjie Ming, Mengfei Zi, Zhijie Liu, Yadong Wang, Biyun Qi, Zhen Ding, Jun Xu, Zhenlin Luo, Xingsen Gao, Shuhong Xie,* Peng Gao,* and Jiangyu Li**

Magnetic materials and devices that can be folded and twisted without sacrificing their functional properties are highly desirable for flexible electronic applications in wearable products and implantable systems. In this work, a high-quality single crystalline freestanding Fe_3O_4 thin film with strong magnetism has been synthesized by pulsed laser deposition using a water-dissolvable $Sr_3Al_2O_6$ sacrificial layer, and the resulting freestanding film, with magnetism confirmed at multiple length scales, is highly flexible with a bending radius as small as 7.18 μm and twist angle as large as 122°, in sharp contrast with bulk magnetite that is quite brittle. When transferred to a polydimethylsiloxane support layer, the Fe_3O_4 film can be bent with large deformation without affecting its magnetization, demonstrating its robust magnetism. The work thus offers a viable solution for flexible magnetic materials that can be utilized in a range of applications.

1. Introduction

Materials and devices that can be folded and twisted without sacrificing their functional properties are highly desirable for flexible electronic applications in wearable products and implantable systems,[1,2] including biosensors,[3] soft robots,[4] and artificial neural interfaces.[5] While much effort has been devoted to developing flexible electronic materials in the last decade,[6,7] it is equally important to advance flexible magnetic materials for data storage, biosensing, and magnetic manipulation. In this regard, magnetite with an inverse spinel structure,[8] Fe_3O_4, is attractive for various applications, which has good ferrimagnetic properties with high Curie temperature,[9] 100% theoretical spin polarization near Fermi level,[10,11] good electric conductivity,[12] and excellent biocompatibility.[13] Nevertheless, achieving flexibility for magnetic materials in general and Fe_3O_4 in particular is quite challenging. Previous studies embedded Fe_3O_4 nanoparticles into soft membranes to achieve flexibility,[14,15] though their magnetic properties are inevitably diluted in nonmagnetic matrix. Fe_3O_4 nanowire arrays and thin films have been grown on various flexible substrates[16–18] including polymers and muscovite mica, though the integration of inorganic magnetic materials on organic polymers is not straightforward, while mica substrate is also difficult to extend or twist. Indeed, there is still strong demand for flexible materials with robust magnetism that can also be twisted and extended, and freestanding films without substrate constraint offer a viable solution to achieve these goals.

F. An, W. Ming, M. Zi, Prof. S. Xie
School of Materials Science and Engineering
Xiangtan University
Xiangtan 411105, China
E-mail: shxie@xtu.edu.cn

F. An, Dr. K. Qu, Prof. G. Zhong, Dr. Y. Dong, W. Ming, M. Zi, B. Qi, Prof. Z. Ding, Prof. J. Li
Shenzhen Key Laboratory of Nanobiomechanics
Shenzhen Institutes of Advanced Technology
Chinese Academy of Sciences
Shenzhen 518055, China
E-mail: gk.zhong@siat.ac.cn; jy.li1@siat.ac.cn

Dr. K. Qu, J. Xu, Prof. P. Gao
Electron Microscopy Laboratory
School of Physics
Peking University
Beijing 100871, China
E-mail: p-gao@pku.edu.cn

Dr. Y. Dong, Z. Liu, Prof. Z. Luo
National Synchrotron Radiation Laboratory
University of Science and Technology of China
Hefei 230029, China

Y. Wang, Prof. X. Gao
Institute for Advanced Materials
South China Academy of Advanced Optoelectronics
South China Normal University
Guangzhou 510006, China

Prof. J. Li
Department of Materials Science and Engineering
Southern University of Science and Technology
Shenzhen, Guangdong 518055, China

The ORCID identification number(s) for the author(s) of this article can be found under https://doi.org/10.1002/adfm.202003495.

DOI: 10.1002/adfm.202003495

Freestanding films are generally achieved in 2-D materials or complex oxides via lift-off process,[19,20] which is only applicable to a limited range of material systems and is prone to failure. In recent years, water-soluble $Sr_3Al_2O_6$ (SAO) as a sacrificial buffer layer has emerged as a powerful solution to process freestanding films with excellent crystalline quality.[21–24] Pioneered by Lu et al. in 2016,[21] the process has now been applied to synthesize a variety of oxide thin films,[22,23] heterostructures,[24] and superlattices,[21] making it possible for us to fabricate freestanding magnetic films as well. In this work, a high-quality single crystalline freestanding Fe_3O_4 thin film with strong magnetism has been synthesized by pulsed laser deposition (PLD) using a water-dissolvable SAO sacrificial layer. The freestanding Fe_3O_4 film, with magnetism confirmed by Lorentz transmission electron microscopy (LTEM), is highly flexible with bending radius as small as 7.18 µm, and can be easily twisted up to 122°. These films are in sharp contrast with bulk magnetite that is quite brittle.[25] When transferred to polydimethylsiloxane (PDMS) support layer, Fe_3O_4 film can be bent with radius as small as 4 mm without affecting its remnant magnetization and coercive field, demonstrating its reversible and robust control of magnetism under large bending deformation.

2. Results

Flexible Fe_3O_4 thin film was designed and processed as schematically illustrated in **Figure 1**a, with the fabrication process consisting of film deposition and transfer. First, SAO sacrifice layer [21] and Fe_3O_4 film were deposited one by one on (001)-oriented $SrTiO_3$ (STO) substrate as detailed in Experimental section, forming STO/SAO/Fe_3O_4 heterostructure. Here the oxygen pressure for growing SAO and Fe_3O_4 was carefully chosen of about 3×10^{-6} Torr to ensure the coherent growth of heterostructure. Then, PDMS with good elastomeric and chemical stability[26,27] was pasted on the top of STO/SAO/Fe_3O_4 heterostructure, serving as a support layer to maintain the integrity of Fe_3O_4 thin film after separation. Finally, the STO/SAO/Fe_3O_4/PDMS stack was immersed into deionized water for approximately 5 min to dissolve the SAO sacrificial layer, separating Fe_3O_4 from STO substrate and transferring it to PDMS. The resulting structure is highly flexible, as demonstrated by the photograph of a bended Fe_3O_4 thin film on the PDMS support layer shown in Figure 1b. The crystallinity of STO/SAO/Fe_3O_4 heterostructure as deposited and PDMS/Fe_3O_4 after it is transferred from STO substrate are verified by X-ray diffraction (XRD) as shown in Figure 1c. In the as-deposited STO/SAO/Fe_3O_4 heterostructure, (00j) reflections from SAO (j = 4, 8, 12) and (kkk) reflections from Fe_3O_4 (k = 1, 2, 3, 4) are evident along with (00i) reflection from STO (i = 1, 2, 3), indicating preferential orientation growth of SAO (001) and Fe_3O_4 (111) on STO (001) substrate with good crystallinity. No impurity phase or reflection from other orientations is detected. After transferring Fe_3O_4 from STO substrate to a PDMS support layer, only (kkk) reflections from Fe_3O_4 (k = 1, 2, 3, 4) remains, demonstrating clean separation of Fe_3O_4 film from STO substrate with the SAO sacrifice layer completely dissolved. This is also confirmed by reciprocal space mapping (RSM) around the (222) diffraction peak of Fe_3O_4 (Figure 1d), exhibiting a clear single peak with no impurities. The lattice constant of Fe_3O_4

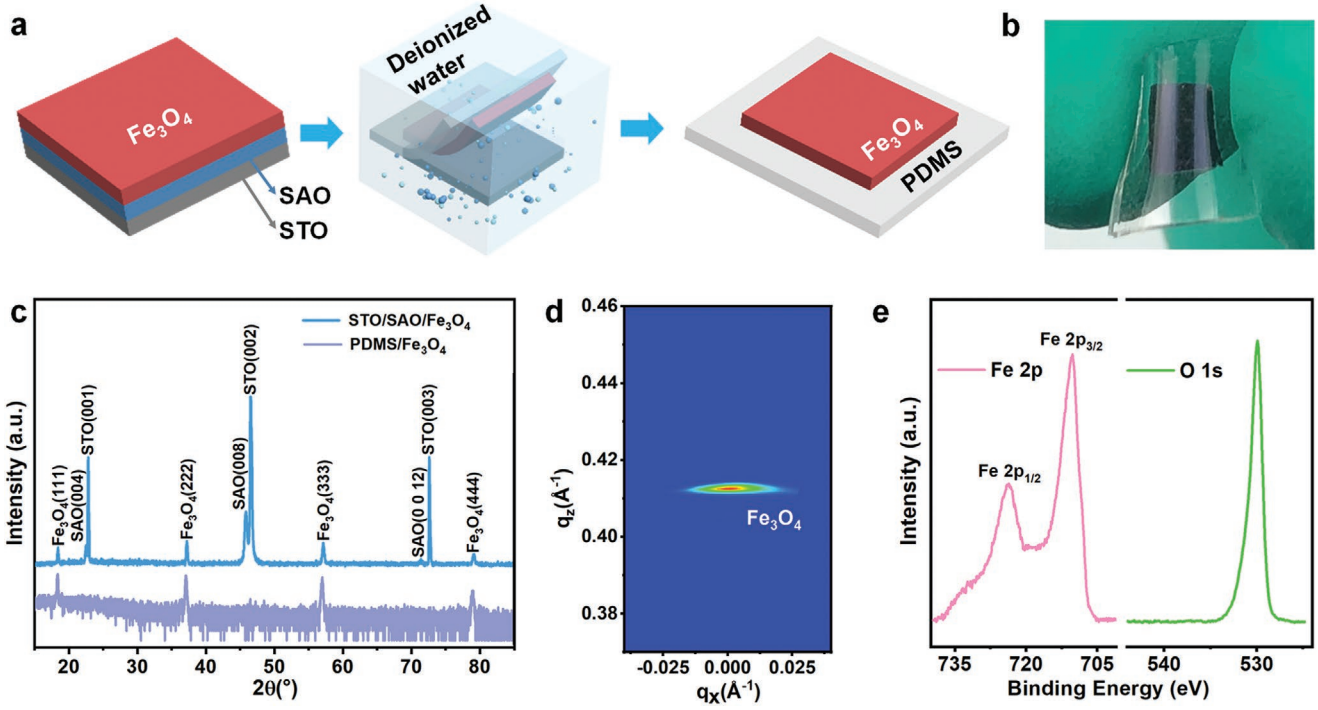

Figure 1. Preparation and structure of freestanding magnetite film. a) The schematic of freestanding Fe_3O_4 thin film preparation, including PLD of SAO and Fe_3O_4 heterostructure on STO substrate, and immersing STO/SAO/Fe_3O_4/PDMS in water to dissolve SAO sacrifice layer, resulting in transferring of freestanding Fe_3O_4 thin film on PDMS separated from STO substrate. b) A photograph of bended PDMS/Fe_3O_4 demonstrating its flexibility. c) XRD patterns of STO/SAO/Fe_3O_4 as deposited and flexible PDMS/Fe_3O_4 after transferring. d) RSM of PDMS/Fe_3O_4 around (222) peak of Fe_3O_4. e) The XPS spectra of STO/SAO/Fe_3O_4 showing Fe_{2p} doublets and O_{1s}.

is estimated from XRD as c = 8.394 Å, consistent with bulk Fe_3O_4.[28] We have also verified the chemical composition of STO/SAO/Fe_3O_4 by high resolution X-ray photoelectron spectroscopy (XPS) in Figure 1e, wherein Fe $2p_{1/2}$ and Fe $2p_{3/2}$ peaks at 723.6 and 710.4 eV correspond to Fe^{3+} and Fe^{2+}, respectively,[29] along with O_{1s} peak at 529.9 eV for O^{2-}. The wide scan XPS spectrum is presented in Figure S1, Supporting Information. These structural characterizations thus confirm the high-quality phase pure Fe_3O_4 thin film we obtained, which can be made freestanding and flexible by dissolving a sacrifice SAO layer.

The morphology and composition of STO/SAO/Fe_3O_4 heterostructure was also examined by atomic force microscopy (AFM), scanning electron microscopy (SEM), and energy-dispersive spectroscopy (EDS) as shown in Figure S2(a-e), Supporting Information, illustrating smooth surface with a root mean square roughness of 992 pm and uniform elemental distributions of iron and oxygen. Low magnification scanning transmission electron microscopy (STEM) image in **Figure 2**a reveals sharp interfaces between homogeneous Fe_3O_4, SAO, and STO layers, with the thicknesses of Fe_3O_4 and SAO estimated to be ≈160 and ≈90 nm, respectively. This is also confirmed by the cross-sectional EDS mappings of Fe, Sr, Al, and Ti elements in Figure 2b–e, revealing their uniform distribution without noticeable interfacial diffusion between Fe_3O_4 and SAO layers. The high-angle annular dark-field (HAADF) STEM image in Figure 2f shows a coherent and clean interface between SAO and Fe_3O_4 at an atomic scale along with the atomic homogeneity of SAO that matches its schematic superstructure of perovskite,[30] though the SAO and Fe_3O_4 layers cannot be simultaneously in focus in a single image. We thus acquired the zoom-in HAADF-STEM images of Fe_3O_4 in Figure 2g, illustrating its atomic homogeneity that matches the schematic inverse spinel structure of Fe_3O_4.[28] Based on the XRD and STEM data, we conclude high-quality epitaxial growth of STO/SAO/Fe_3O_4 heterostructure, with the epitaxial relationships determined as STO [001]//SAO [001]//Fe_3O_4 [111]. Considering Fe_3O_4 with a = b = c = 8.394 Å and $Sr_3Al_2O_6$ with a = b = c = 15.844 Å, it can be determined that $4\sqrt{2}$ Fe_3O_4 cells match 3 $Sr_3Al_2O_6$ cells at the interface, as schematically shown in Figure S3, Supporting Information, corresponding to a tensile strain of 0.12% for as-grown Fe_3O_4.

The magnetic properties of Fe_3O_4 thin films fabricated were investigated at macroscopic, mesoscopic, and microscopic

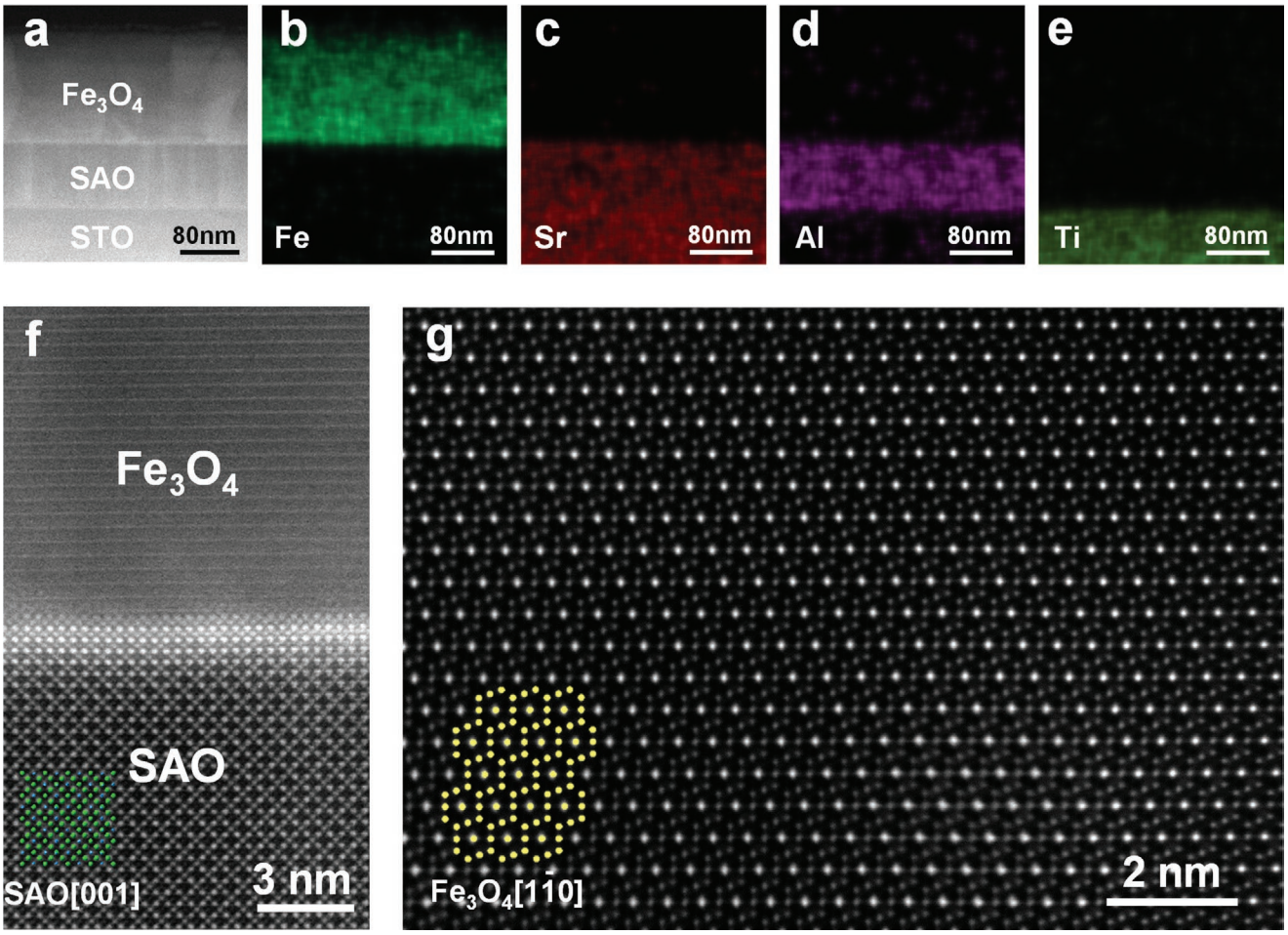

Figure 2. Microstructure of STO/SAO/Fe_3O_4 heterostructure. a) Low-resolution cross-section STEM image of STO/SAO/Fe_3O_4. b–e) EDS element mapping of STO/SAO/Fe_3O_4. f) Atomic resolution HAADF-STEM image at SAO/Fe_3O_4 interface with SAO crystalline model viewed along [001] direction while Fe_3O_4 is slightly out of focus. g) Zoom-in HAADF-STEM image of Fe_3O_4 with crystalline model viewed along [$1\bar{1}0$] direction.

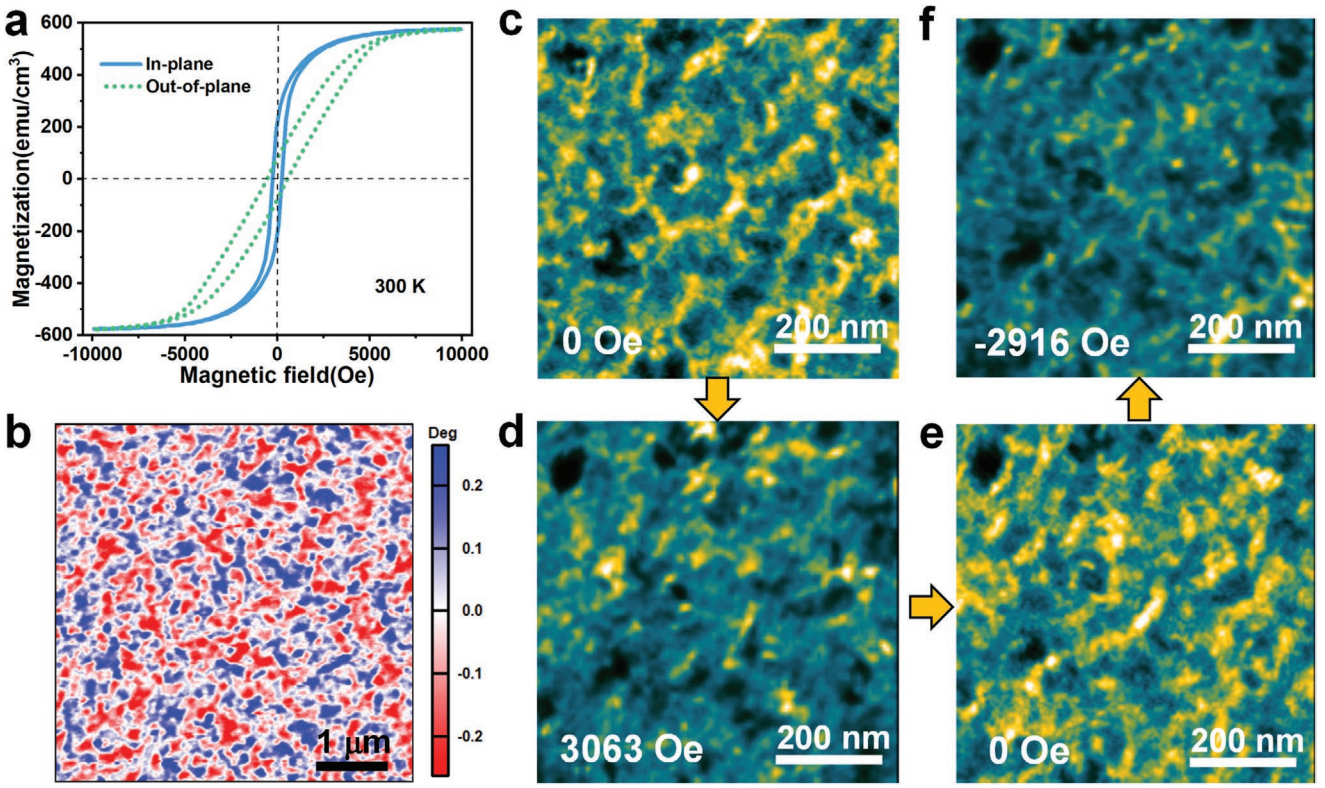

Figure 3. Magnetic properties of Fe_3O_4 thin film cross scales. a) IP and OOP magnetic hysteresis (M-H) loops of as-grown Fe_3O_4 thin film on STO/SAO. b) MFM phase mapping of as-grown Fe_3O_4 thin film on STO/SAO. c–f) LTEM images of freestanding Fe_3O_4 thin film, showing magnetic domain evolution under external magnetic fields of c) 0 Oe, d) 3063 Oe, e) 0 Oe, and f) −2916 Oe. The yellow contrast corresponds to the domain walls. The up-left dark feature is used as the reference to track the same region.

scales as shown in **Figure 3**. The macroscopic magnetic hysteresis (M-H) loops of as-grown Fe_3O_4 on STO/SAO measured along the in-plane (IP) and out-of-plane (OOP) directions at room temperature are presented in Figure 3a, confirming typical magnetic characteristics with saturated magnetization (M_s) of ≈570 emu cm^{-3} under an external magnetic field of 10 000 Oe. The coercive field (H_c) extracted from zoomed-in M-H loops (Figure S4, Supporting Information) is estimated to be ≈250 Oe for IP and ≈530 Oe for OOP, while the corresponding remnant magnetizations are ≈215 emu cm^{-3} and ≈80 emu cm^{-3}, respectively. The magnetic easy axis is found to be IP due to shape anisotropy, while the bulk magnetite crystal has easy axis along < 111>.[31] At the mesoscopic scale, magnetic force microscopy (MFM) was employed as shown in Figure 3b, where phase mapping reveals the random distribution of magnetic domains in the as-grown Fe_3O_4 thin film on STO/SAO. These magnetic domains can be manipulated by IP magnetic field applied (Figure S5, Supporting Information), confirming the magnetic nature of the domains observed. By directly transferring a freestanding Fe_3O_4 thin film onto Cu TEM grid without using PDMS support layer (Figure S6, Supporting Information), microscopic LTEM images of freestanding Fe_3O_4 under different external magnetic fields were obtained. In Fresnel mode [32,33] of LTEM, bright and dark contrasts arise from magnetic domain walls, and these are what we observe in Figure S7, Supporting Information, especially those highlighted by orange boxes. Bright stripes are observed in under-focus condition, which transit into dark stripes in over-focus condition, while these stripes disappear altogether under in-focus condition, indicating that they are indeed magnetic domain walls. More importantly, as can be seen in Figure 3c–f, many domain walls, as indicated by yellow stripes in under-focus condition, disappear under either positive or negative magnetic fields around 3000 Oe, while they reemerge when the field is reduced to zero, illustrating the evolution of magnetic structure under external field that is consistent with macroscopic M-H loops. The LTEM images under different magnetic fields over larger area covering this regions are shown in Figure S8, Supporting Information. These observations confirm robust magnetism in freestanding Fe_3O_4 that can be reversibly controlled by external magnetic field, which is critical for their flexible spintronics applications.

One of the key advantages of freestanding films is their flexibility, ideal for various device applications. To verify this, we have also collected freestanding Fe_3O_4 thin film on Cu grid, and cut a flake of freestanding Fe_3O_4 by focused ion beam (FIB). One end of the freestanding Fe_3O_4 flake was fixed on the Cu grid by carbon coating, and other end was welded with a tungsten probe by carbon coating for in-situ SEM manipulation. Bending test was first carried out as shown in **Figure 4**a–d. The flat Fe_3O_4 flake in Figure 4a was pushed by the attached tungsten probe from left to right end, resulting in overall downward bending seen in Figure 4b,c, though a small portion of upward bending near the probe is also observed. The smallest down-

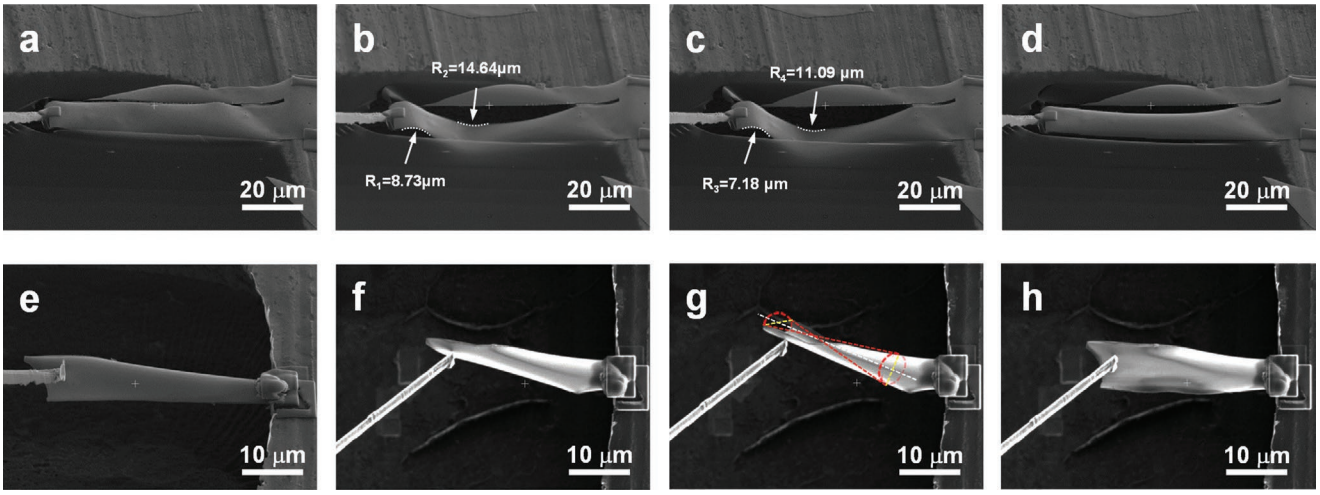

Figure 4. Flexibility of freestanding Fe_3O_4 thin film. a–d) SEM images of freestanding Fe_3O_4 thin film under bending. e–h) SEM images of freestanding Fe_3O_4 thin film under twisting.

ward bending radius is estimated to be R_2 = 11.09 μm in Figure 4c, while the smallest upward bending radius is as small as 7.18 μm in Figure 4c, corresponding to bending strain of ≈0.72% and ≈1.11%, respectively, calculated using film thickness of ≈160 nm. Importantly, there are no damages experienced during this complex bending process, and the freestanding Fe_3O_4 flake fully recovers its initial flat state as seen in Figure 4d when we withdraw the fixed tip from right to left end. In addition, we have tried to twist the freestanding flake as shown in Figure 4e–h, where it is observed that the torsional angle can gradually increase to as large as 122° (Figure 4g), after which it fully recovers its initial state (Figure 4h) as well upon unloading. These results reveal the outstanding flexibility and mechanical strength of freestanding Fe_3O_4 thin film, though the bulk magnetite is brittle with uneven fracture.[25] Movies for these in-situ bending and twisting are given in Movies S1 and S2, Supporting Information, and additional flexibility testing data are presented in Figure S9, Supporting Information.

We then examine the stability of magnetization in flexible Fe_3O_4 thin film under bending. As shown in **Figure 5**a,b, both

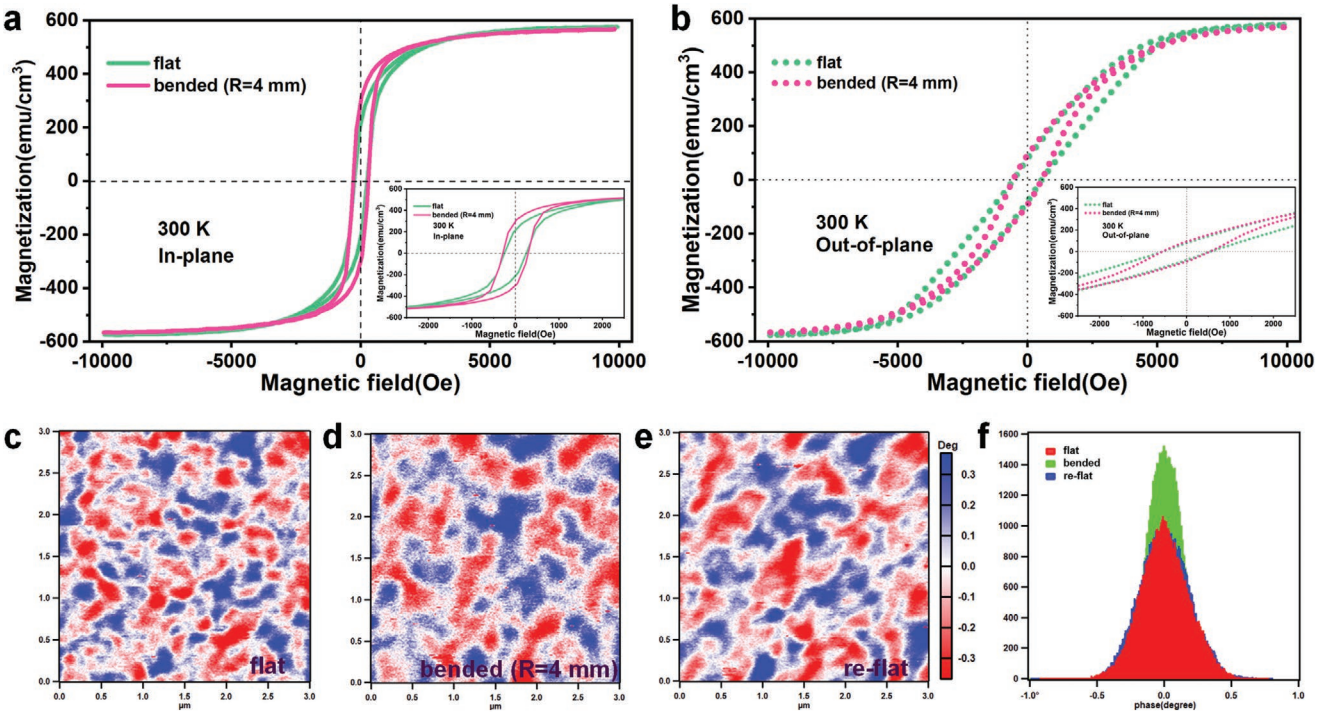

Figure 5. Magnetic properties of freestanding Fe_3O_4 thin film under bending. a) IP and b) OOP M-H loops of PDMS/Fe_3O_4 thin film in flat and bended (R = 4 mm) configurations. c–e) MFM phase mappings of Fe_3O_4 thin film in c) flat, d) bended (R = 4 mm), and e) re-flat configurations. f) Histogram distributions of MFM phase in flat, bended, and reflat configuration.

IP and OOP M-H loops of PDMS/Fe_3O_4 experience notable yet insignificant changes when it transit from flat to bended configuration with upward bending radius as small as 4 mm. The thickness of PDMS is about 50 μm, and thus the tensile strain induced in Fe_3O_4 is estimated to be 0.625%. It is observed that both M_s and H_c remain stable, and the remnant IP magnetization becomes slightly larger under bending, suggesting that the bending deformation tends to stabilize IP magnetization due to induced tensile stress. Even smaller difference are seen in OOP M-H loops, for which remnant magnetization is also unaffected by bending. As such, bending does not seem to affect magnetic easy axis under our experimental condition, though the effect on magnetic anisotropy under larger bending deformation has been reported.[18] Another key feature of Fe_3O_4 is Verwey transition,[34] and earlier study showed that it also is not sensitive to bending on mica substrate.[18] To appreciate the effect of mechanical deformation at the microscopic scale, we also recorded the evolution of MFM mappings under different bending, as shown in Figure 5c-e. The MFM phase mapping of flat Fe_3O_4 thin film shows strayed magnetic domains (Figure 5c), which grows slightly larger under a bending radius 4 mm (Figure 5d), illustrating modest magnetoelastic interactions. After bending deformation was released, the magnetic domains change yet do not recover their original pattern (Figure 5e). Nevertheless, the histogram distributions in Figure 5f show that statistically there is little difference among three different configurations, especially between flat and reflat state. For bended film, the phase distribution is found to be more concentrated. The AFM topography mappings corresponding to Figure 5c–e are presented in Figure S10, Supporting Information, confirming the evolution of magnetic domain was recorded in the same region. Additional MFM data under bending show similar behavior, as presented in Figure S11, Supporting Information. These macroscopic and microscopic results confirm that our flexible Fe_3O_4 thin film enjoys robust magnetic properties.

3. Conclusions

In summary, STO/SAO/Fe_3O_4 heterostructure was fabricated by PLD and freestanding Fe_3O_4 thin film has been obtained by dissolving the sacrificial layer of SAO, with both as-deposited and freestanding Fe_3O_4 films exhibiting high-quality single crystallinity. The freestanding Fe_3O_4 thin film demonstrates outstanding mechanical flexibilities with bending radius as small as 7.18 μm and twist angle as large as 122° without damage, while robust magnetism is well maintained under such large bending deformation. The work thus offers a viable solution for flexible magnetic materials that can be utilized in a range of applications.

4. Experimental Section

Preparation of STO/SAO/Fe_3O_4 epitaxial heterostructure: The SAO sacrificial layer was first epitaxially grown on STO (001) substrate by PLD with a 248 nm wavelength KrF excimer laser at 700 °C and oxygen pressure at 3×10^{-6} Torr. After SAO deposition, the SAO film was cooled to 400 °C with a rate of 25 °C/min at the oxygen pressure of 3×10^{-6} Torr, and then Fe_3O_4 layer was epitaxially grown at 400 °C with the oxygen pressure of 3×10^{-6} Torr. The target-substrate distance was 8 cm, and the laser energy was about 300 mJ with a laser pulse rate of 10 Hz. After Fe_3O_4 deposition, the STO/SAO/Fe_3O_4 epitaxial heterostructure was slowly cooled down to room temperature with a rate of 25 °C/min.

Preparation of flexible and freestanding Fe_3O_4 epitaxial thin film: First, the PDMS support layer was covered on the surface of STO/SAO/Fe_3O_4 heterostructure and the PDMS/Fe_3O_4/SAO/STO sample was heated for 10 min at 90 °C, ensuring the interface between PDMS and Fe_3O_4 has a tight fit. Then, immersing the sample into the deionized water to dissolve the SAO sacrificial layer, a flexible PDMS/Fe_3O_4 thin film can be obtained after about 5 min. Regarding to the freestanding Fe_3O_4 thin film for LTEM characterization and SEM bending tests, a holey carbon Cu grid was chosen to support freestanding Fe_3O_4 epitaxial thin film instead of PDMS.

Structure and magnetic properties characterizations: The crystalline structure of STO/SAO/ Fe_3O_4 heterostructure and PDMS/Fe_3O_4 film were studied by X-ray diffraction (XRD, Rigaku SmartLab X-ray diffractometer) and Reciprocal space mapping (RSM) using a high-resolution synchrotron X-ray, 1W1A Beamline of the Beijing Synchrotron Facility (BSRF). Atomic-resolution high-angle annular dark-field (HAADF) STEM was obtained through an aberration-corrected Titan themis G2 operated at 300 kV equipped with energy dispersive X-ray spectroscopy (EDS) detectors (Super-X). The macroscopic magnetic property was conducted by a physical property measurement system (PPMS, Quantum Design, model 6000), the mesoscopic magnetic properties were characterized by magnetic force microscopy (MFM, Asylum Research MFP-3D-Bio). The ASYEMFM magnetic probe with 400 Oe coercive field and ASYMFMHC magnetic probe with a high coercive field (>5000 Oe) were used for MFM mapping. Both M-H- and MFM-involved bending experiments were carried out by transferring the flexible PDMS/Fe_3O_4 film to a 3-D printed hemispherical sphere with radius of curvature of 4 mm, whose schematic image was shown in Figure S12, Supporting Information. And microscopic magnetic properties was operated by LTEM (Thermal Fisher Titan themis G2) on Fresnel mode. In-situ TEM bending and recovery test of freestanding Fe_3O_4 thin film was conducted by FIB (Thermal Fisher Helios G4) with Omniprobe.

Supporting Information

Supporting Information is available from the Wiley Online Library or from the author.

Acknowledgements

This work was supported by the National Natural Science Foundation of China (11627801, 51902337, 51672007, 11974023), National Key Research and Development Program of China (2016YFA0201001), Shenzhen Science and Technology Innovation Committee (KQTD20170810160424889, JCYJ20170818163902553, JCYJ20170818155813437) and Hunan Provincial Innovation Foundation for Postgraduate (CX20190475).

Conflict of Interest

The authors declare no conflict of interest.

Authors Contributions

F.A., K.Q. and G.K.Z. contributed equally to this work. The project was conceived and coordinated by J.Y.L and G.K.Z. The films were synthesized by F.A. and M.F.Z. under the guidance of J.Y.L., G.K.Z., and S.H.X. XRD, SEM, and XPS were carried out and analyzed by F.A., M.F.Z., and W.J.M. XRD and RSM was carried out and analyzed by Y.Q.D., Z.J.L., F.A., and Z.L.L. TEM and in-situ SEM were carried out and analyzed by

K.Q., J.X., F.A., G.K.Z., and P.G Macro- and micro-magnetic performance were carried out and analyzed by Y.D.W., X.S.G., K.Q., F.A., G.K.Z. and P.G. B.Y.Q. and Z.D. printed the 3-D hemispherical sphere for AFM testing. J.Y.L., G.K.Z., and F.A. wrote the manuscript, and all the authors participated in discussions and analysis.

Keywords

flexible spintronics, freestanding films, magnetism, magnetite

Received: April 21, 2020
Revised: May 10, 2020
Published online: May 28, 2020

[1] W. Gao, S. Emaminejad, H. Y. Y. Nyein, S. Challa, K. Chen, A. Peck, H. M. , Fahad, H. Ota, H. Shiraki, D. Kiriya, D.-H. Lien, G. A. Brooks, R. W. Davis, A. Javey, *Nature* **2016**, *529*, 509.
[2] S. Huang, Y. Liu, Y. Zhao, Z. Ren, C. F. Guo, *Adv. Funct. Mater.* **2019**, *29*, 1805924.
[3] J. Kim, A. S. Campbell, B. E.-F. de Ávila, J. Wang, *Nat. Biotechnol.* **2019**, *37*, 389.
[4] A. Rafsanjani, K. Bertoldi, A. R. Studart, *Sci. Rob.* **2019**, *4*, eaav7874.
[5] M. A. Hejazi, W. Tong, A. Stacey, A. Soto-Breceda, M. R. Ibbotson, M. Yunzab, M. I. Maturana, A. Almasi, Y. J. Jung, S. Sun, H. Meffin, J. Fang, M. E. M. Stamp, K. Ganesan, K. Fox, A. Rifai, A. Nadarajah, S. Falahatdoost, S. Prawer, N. V. Apollo, D. J. Garrett, *Biomaterials* **2020**, *230*, 119648.
[6] H.-R. Lim, H. S. Kim, R. Qazi, Y.-T. Kwon, J.-W. Jeong, W.-H. Yeo, *Adv. Mater.* **2019**, 1901924.
[7] G. Zhong, J. Li, *J. Materiomics* **2020**, *6*, 455.
[8] G. Zhong, F. An, Y. Bitla, J. Wang, X. Zhong, J. Yu, W. Gao, Y. Zhang, C. Tan, Y. Ou, J. Jiang, Y.-H. Hsieh, X. Pan, S. Xie, Y.-H. Chu, J. Li, *ACS Nano* **2018**, *12*, 9558.
[9] P. A. Miles, W. B. Westphal, A. V. Hippel, *Rev. Mod. Phys.* **1957**, *29*, 279.
[10] S. F. Alvarado, W. Eib, F. Meier, D. T. Pierce, K. Sattler, H. C. Siegmann, *Phys. Rev. Lett.* **1975**, *34*, 319.
[11] T. L. Qu, Y. G. Zhao, P. Yu, H. C. Zhao, S. Zhang, L. F. Yang, *Appl. Phys. Lett.* **2012**, *100*, 242410.
[12] E. J. W. Verwey, P. W. Haayman, *Physica* **1941**, *8*, 979.
[13] J. Sun, S. Zhou, P. Hou, Y. Yang, J. Weng, X. Li, M. Li, *J. Biomed. Mater. Res., Part A* **2007**, *80A*, 333.
[14] J. Liang, Y. Xu, D. Sui, L. Zhang, Y. Huang, Y. Ma, F. Li, Y. Chen, *J. Phys. Chem. C* **2010**, *114*, 17465.
[15] Y. Lin, H. Y. Xu, Z. Q. Wanga, T. Cong, W. Z. Liu, H. L. Ma, Y. C. Liu, *Appl. Phys. Lett.* **2017**, *110*, 193503.
[16] M. Zhang, M. Wang, M. Zhang, A. Maimaitiming, L. Pang, Y. Liang, J. Hu, G. Wu, *ACS Appl. Nano Mater.* **2018**, *1*, 5742.
[17] M. S. Ansari, M. H. D. Othman, M. O. Ansari, S. Ansari, M. Z. M. Yusop, *J. Alloys Compd.* **2020**, *816*, 152532.
[18] P. C. Wu, P. F. Chen, T. H. Do, Y.-H. Hsieh, C.-H. Ma, T. D. Ha, K.-H. Wu, Y.-J. Wang, H.-B. Li, Y.-C. Chen, J.-Y. Juang, P. Yu, L. M. Eng, C.-F. Chang, P.-W. Chiu, L. H. Tjeng, Y.-H. Chu, *ACS Appl. Mater. Interfaces* **2016**, *8*, 33794.
[19] H. S. Kum, H. Lee, S. Kim, S. Lindemann, W. Kong, K. Qiao, P. Chen, J. Irwin, J. H. Lee, S. Xie, S. Subramanian, J. Shim, S.-H. Bae, C. Choi, L. Ranno, S. Seo, S. Lee, J. Bauer, H. Li, K. Lee, J. A. Robinson, C. A. Ross, D. G. Schlom, M. S. Rzchowski, C.-B. Eom, J. Kim, *Nature* **2020**, *578*, 75.
[20] Y. Zhang, L. Shen, M. Liu, X. Li, X. Lu, L. Lu, C. Ma, C. You, A. Chen, C. Huang, L. Chen, M. Alexe, C.-L. Jia, *ACS Nano* **2017**, *11*, 8002.
[21] D. Lu, D. J. Baek, S. S. Hong, L. F. Kourkoutis, Y. Hikita, H. Y. Hwang, *Nat. Mater.* **2016**, *15*, 1255.
[22] D. Ji, S. Cai, T. R. Paudel, H. Sun, C. Zhang, L. Han, Y. Wei, Y. Zang, M. Gu, Y. Zhang, W. Gao, H. Huyan, W. Guo, D. Wu, Z. Gu, E. Y. Tsymbal, P. Wang, Y. Nie, X. , Pan, *Nature* **2019**, *570*, 87.
[23] G. Dong, S. Li, M. Yao, Z. Zhou, Y.-Q. Zhang, X. Han, Z. Luo, J. Yao, B. Peng, Z. Hu, H. Huang, T. Jia, J. Li, W. Ren, Z.-G. Ye, X. Ding, J. Sun, C.-W. Nan, L.-Q. Chen, J. Li, M. Liu, *Science* **2019**, *366*, 475.
[24] D. Lu, S. Crossley, R. Xu, Y. Hikita, H. Y. Hwang, *Nano Lett.* **2019**, *19*, 3999.
[25] J. W. Anthony, R. A. Bideaux, K. W. Bladh, M. C. Nichols, *In Handbook of Mineralogy*, Mineralogical Society of America, Chantilly, VA. **2017**, p. 333.
[26] P. Yang, G. Wirnsberger, H. C. Huang, S. R. Cordero, M. D. McGehee, B. Scott, T. Deng, G. M. Whitesides, B. F. Chmelka, S. K. Buratto, G. D. Stucky, *Science* **2000**, *287*, 465.
[27] E. Delamarche, H. Schmid, B. Michel, H. Biebuyck, *Adv. Mater.* **1997**, *9*, 741.
[28] M. E. Fleet, *Acta Crystallogr,. Sect. B Struct. Crystallogr. Cryst. Chem.* **1981**, *37*, 917.
[29] L. Wan, D. Yan, X. Xu, J. Li, T. Lu, Y. Gao, Y. Yao, L. Pan, *J. Mater. Chem. A* **2018**, *6*, 24940.
[30] J. A. Alonso, I. Rasines, J. L. Soubeyroux, *Inorg. Chem.* **1990**, *29*, 4768.
[31] G. W. Fernando, In *Handbook of Metal Physics*, Elsevier, Amsterdam **2008**, *4*, pp. 89–110.
[32] J. N. Chapman, M. R. Scheinfein, *J. Magn. Magn. Mater.* **1999**, *200*, 729.
[33] J. N. Chapman, *Mater. Sci. Eng., B* **1989**, *3*, 355.
[34] Z. Zhang, S. Satpathy, *Phys. Rev. B* **1991**, *44*, 13319.